ACS APPLIED MATERIALS & INTERFACES

Research Article

www.acsami.org

An Open Pit Nanofluidic Tool: Localized Chemistry Assisted by Mesoporous Thin Film Infiltration

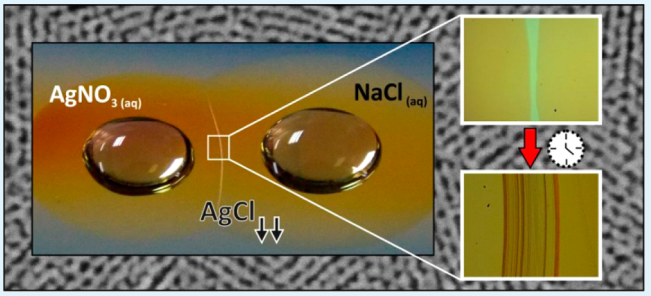
Magalí Mercuri,[†] Karina A. Pierpauli,[†] Claudio L. A. Berli,[*,‡] and Martín G. Bellino[*,†]

[†]Departamento de Micro y Nanotecnología, Comisión Nacional de Energía Atómica, Av. Gral. Paz, 1499 San Martín, Buenos Aires, Argentina

[‡]INTEC (Universidad Nacional del Litoral-CONICET) Predio CCT CONICET Santa Fe, RN 168, 3000 Santa Fe, Argentina

Supporting Information

ABSTRACT: Nanofluidics based on nanoscopic porous structures has emerged as the next evolutionary milestone in the construction of versatile nanodevices with unprecedented applications. However, the straightforward development of nanofluidically interconnected systems is crucial for the production of practical devices. Here, we demonstrate that spontaneous infiltration into supramolecularly templated mesoporous oxide films at the edge of a sessile drop in open air can be used to connect pairs of landmarks. The liquids from the drops can then join through the nanoporous network to guide a localized chemical reaction at the nanofluid−front interface. This method, here named "open-pit" nanofluidics, allows mixing reagents from nanofluidically connected droplet reservoirs that can be used as reactors to conduct reactions and precipitation processes. From the fundamental point of view, the work contributes to unveiling subtle phenomena during spontaneous infiltration of fluids in bodies with nanoscale dimensions such as the front broadening effect and the oscillatory behavior of the infiltration−evaporation front. The approach has distinctive advantages such as easy fabrication, low cost, and facility of scaling up for future development of ultrasensitive detection, controlled nanomaterial synthesis, and novel patterning methods.



KEYWORDS: *mesoporous films, nanofluidics, capillary infiltration, localized chemistry, nanodevices*

INTRODUCTION

Nanofluidics have proved to be a very useful and exciting medium for applications in tasks as diverse as separation, energy conversion, molecular manipulation, and sensing.[1−5] The simplicity of nanofluidic systems promises to be as revolutionary in the coming decades as the miniaturization of microfluidic devices was in the previous ones. A device that consists only of a surface would represent the ultimate limit of simple nanofluidic platforms. In a separate but related thread, chemical reactions at appointed places are becoming increasingly necessary to study biological processes that occur in cellular compartments,[6−8] synthesize novel nanostructures,[9] and achieve combinatorial screening and high-throughput assays.[10] To perform reactions on localized sites and at such dimensions, it is critical to manipulate reagents and control their mixing into well-defined localizations. It is also important to control the dimensions of these reactors and their positioning to facilitate monitoring. We propose here an alternative approach. This approach, named "open-pit" nanofluidics (OPN), obviates the usually costly step of fabricating microdevices and wells: it can be employed to mix reagents from nanofluidically connected droplets that can be used as reservoirs to conduct spacially localized reactions over micrometer-scale regions. In particular, we found that complex filling dynamics in mesoporous oxide thin films (MOTF)[11−13] is ideal for running such nanofluidic processes. In addition, supramolecularly templated MOTF guarantees the control of the porous morphologies that consists in nanoscopic pores connected by smaller necks.[14−16] When a drop is deposited on the surface of a MOTF, the liquid from the droplet reservoir enters the porous substrate and builds an annulus at its periphery.[11,12] Annuli nucleate from two drop landmarks and grow via capillarity at their free boundaries, which infiltrate into the nanoporous film. When these fluid fronts meet, they join, forming a nanofluidic connection. This interesting behavior enables the confined and programmable positioning of chemical reactions from droplet regents by their precise approach through their surrounding rings. This straightforward OPN method comprises only a simple step: microliter droplets deposition on MOTF; then, spontaneous nanofluidic delivery into the porous network is self-produced. It could allow mixture of nanovehiculized reagents directly on the meeting point of the infiltrated annuli from different drops, thus forming well-defined interfaces in which individual reactions can be conducted. In this study, as a proof of concept, we demonstrate that OPN enables performance of the silver chloride

Received: March 2, 2017
Accepted: May 2, 2017
Published: May 2, 2017

 © XXXX American Chemical Society

DOI: 10.1021/acsami.7b03080
ACS Appl. Mater. Interfaces XXXX, XXX, XXX−XXX

precipitation reaction, creating localized chemistry. We believe that this OPN approach could be extrapolated as a desktop tool to synthesize nanomaterials and perform distinct confined (bio)chemical reactions at desired locations and/or create nanofluidic circuits.

RESULTS AND DISCUSSION

Mesoporous titania thin films were produced via a sol−gel method combined with supramolecular self-assembly by dip-coating of silicon substrates using protocols described in the literature.[11,14,15] This led to the formation of mesoporous films (180 nm thick) displaying aligned pore arrays with a conduit-like mesostructure (CLM) (Figure 1a and TableS1); 50% porous and pore and neck sizes of 6 and 4.1 nm, respectively, as indicated by electron microscopy and environmental ellipsometric porosimetry (EEP).[17]

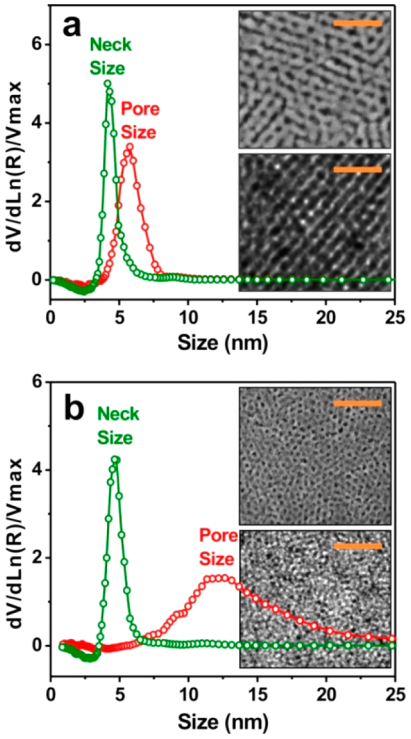


Figure 1. Mesoporous thin film characterization. Pore size distribution (red line) and neck size distribution (green line) of typical conduit-like (a) and locally ordered (b) mesostructures. Upper and lower insets are, respectively, SEM and TEM micrographs of each mesoporous film. Scale bar = 100 nm.

Previous studies suggested that at 23 °C and 46% relative humidity, capillary ring grows efficiently from sessile water drops.[11] Under these conditions, we evaluated the OPN method for creating well-defined mixture sites and subsequently using them to confine the synthesis of materials on surfaces. We then localized the well-known $Ag^+ + Cl^- \rightarrow AgCl \downarrow\downarrow$ reaction by depositing microliter drops of 1 M sodium chloride (NaCl) and 0.1 M silver nitrate ($AgNO_3$) solutions separated by 10 mm on the mesoporous films (Figures 2a and b). Annuli grew from both drops and increased in length gradually via capillary imbibition up to meet each other. The annuli can be clearly seen because the wetted region produces a refractive index contrast in relation to the outer dry zone. Interestingly, this assay produced precipitation reactions only within the contact annulus interface, making it possible to visualize the abrupt precipitation process using optical microscopy (see Movie S1 in the Supporting Information). We captured, in addition, representative snapshots of the localized reaction process at different times (Figure 2c). These observations showed the proper localization of silver chloride (AgCl) precipitation through the nanocapillary communication of the different drop reservoirs, thus demonstrating the capability of the OPN method for localizing chemical reactions at the nanofluidic connection. The juncture shown in Figure 2c is representative of the definitive narrow line marked under this condition. This dark line corresponds to a local increase in the film refractive index due to the presence of precipitates.

We next studied how annuli grew and formed the interface reaction at varied NaCl concentrations. As a preliminary step, we estimated the change of the capillary imbibition rate with NaCl concentration where, for example, an increase in infiltration rate as large as 3.5 times can be observed in the concentration range between 0.1 and 1 M. Furthermore, a significant increase in the fluid−front traveled distance with respect to pure water,[11] was also observed. Thus, these data provide evidence that a new balance between infiltration−evaporation in the solutions regarding pure water is a viable approach to controlling capillary fluid front displacement. The influence of salt concentration can be rationalized in the framework of the model reported in our previous work,[11] where the infiltration rate results from the balance between capillary filling and liquid evaporation. It is known that the evaporation rate of NaCl solutions in porous media decreases with salt concentration (around 40% for 1 M at room temperature),[18] following the diminution of the activity of aqueous solutions.[19] As evaporation counterbalances capillary filling, increasing salt concentration has two simultaneous effects: a faster infiltration rate and a larger annulus width (see ref 11 for further details). Nevertheless, the substantial augmentation of infiltration rate observed in practice (more than three times that relative to pure water) suggest an additional cause, probably associated with an increase in the porous matrix permeability with ionic strength, which is an interesting feature that deserves further research in MOTF. Finally, mixing different reactant concentrations in the annuli junction enabled the formation of localized reactions. The precipitate zones observed display an extended linear structure, as shown in Figure 3. However, both the width of the reaction zone and the reaction time were found to depend on NaCl concentration (Figure 3a). The lower salt concentrations lead to a wider precipitation zone (nearly 500 μm for NaCl 0.01 M; Figure 3b) as well as the longer reaction times (around 450 s). Figure 3c shows the features commonly observed for intermediate salt concentrations (around 240 μm width; 160 s of reaction time). Figure 3d presents the reaction zone for the higher NaCl concentration employed, which displays a noteworthy degree of narrowness (around 15 μm definitive width), consequently with reaction times of a few seconds. Furthermore, Figure 3e presents results of quantitative energy dispersive X-ray spectroscopy (EDS) microanalysis of the linear structures, which confirms the presence of both Ag and Cl along the junction zone.

Although the method was designed to generate linear chain-like structures formed by chemical reaction at the time of contact, we expected to (and finally did) observe an early precipitation (before the visible annuli come into contact) for some mesoporous film morphologies because of the front

DOI: 10.1021/acsami.7b03080
ACS Appl. Mater. Interfaces XXXX, XXX, XXX−XXX

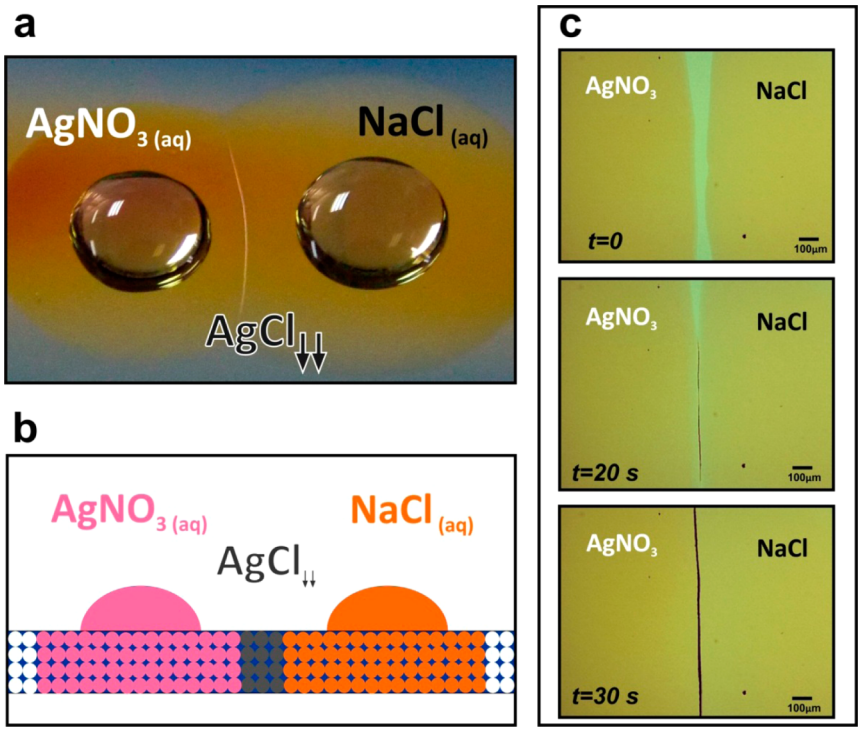


Figure 2. Nanofluidic delivery and localizing capabilities of OPN. (a) Picture of two sessile droplets of $AgNO_3$ (left) and NaCl (right) exhibiting the characteristic AgCl white line arising from localized reaction at the boundary between annuli (interdroplet distance = 10 mm). (b) Schematic illustration of the OPN method showing the positioning of two droplets, followed by precise nanodelivery of reactants through the film for subsequent mixing at the meeting line. (c) Time-lapse optical microscopy sequence showing the initial reaction stage (t = 0) when the nanofluidic connection is established between the annuli (t = 20 s) and when the final state is attained (t = 30 s).

roughening that takes place during spontaneous imbibition in porous media.[20−23] In fact, Figure 4b and Movie S2 in the Supporting Information show that AgCl precipitation occurs long before the (optically detected) fluid fronts connect each other. This is due to the fact that the (optically observed) fluid front is preceded by an unsaturated zone, the width $w(t)$ of which enlarges with time t.[22,23] The effect is schematically shown in Figure 4c, where the liquid volume fraction in the film is drawn as a function of the position of the advancing front: behind the visible boundary, the pore space is completely filled with fluid (saturated); ahead the visible boundary, the pore space is partially filled (unsaturated), and beyond that transition zone, the pore space is empty (filled with air plus a certain water content in equilibrium with ambient vapor pressure). The relevant aspect is that the fluid front, instead of being a step-like function in water content, consists in a smooth transition from fully saturated to empty pores.

It is worth mentioning that we have not specifically measured the front broadening of the liquid−air interface; additional studies are necessary to explore this subtle effect in mesoporous films. Conversely, we uncover here this phenomenon through the OPN set up. In fact, Figure 4b provides evidence that the optically invisible roughening of the imbibition fronts actually takes place in MOTF, being clearly manifest in this locally ordered mesostructure (LOM) (see Figure 1b and Table S1 for mesostructure details). Furthermore, Movie S2 shows how the front broadening effects depend on ionic strength and perhaps on the particular ionic species as well. Because the precipitation line develops closer to the NaCl solution front, one may conclude that the unsaturated region is substantially larger for 0.1 M $AgNO_3$ than for 1 M NaCl.

Figure 4a illustrates the case of CLM, where the front broadening effect is much more subtle and a priori hidden (see also Movie S1); however, it plays an important role in defining the shape and size of the precipitation zone, as discussed in the paragraph below. Concerning the influence of the microscopic geometry, it has been recently shown that the hydrodynamic permeability of mesoporous films decreases with pore radius for a given neck size.[12] In addition, we found that the rate of spontaneous imbibition is inversely proportional to the cubed ratio of largest to the smallest pore radius.[13] Now, after the experimental results reported here, one may add that the front roughening effect is more pronounced for the highest ratio of pore to neck size. Effectively, the comparison of Figures 4a and b suggest that the imbibition in LOM presents a liquid−air interface broader than that of CLM, in correlation with a larger ratio of pore to neck size, according to Figures 1a and b, respectively.

Now one may come back to Figure 3 to interpret the reaction times and the final width of precipitation zones. First, it is considered that a certain degree of front broadening exists in CLM, which can be inferred after a close inspection of Figure 2c at t = 20s. Besides, it is reasonable to assume that the salt solution with the slowest infiltration rate (smaller ionic strength) develops the broadest front (largest w), also considering that the elapsed time to join the fluid front coming from the next droplet is relatively larger. In this scenario, the 1 M NaCl solution presents the narrowest front (smallest w), and when it meets the silver solution, the precipitation of AgCl forms a line along the boundary between annuli (Figure 3d). In the case of 0.1 M NaCl solution, the front is smoother, involving a preceding zone of unsaturated material. When this front meets that of the silver solution, both fronts are

DOI: 10.1021/acsami.7b03080
ACS Appl. Mater. Interfaces XXXX, XXX, XXX−XXX

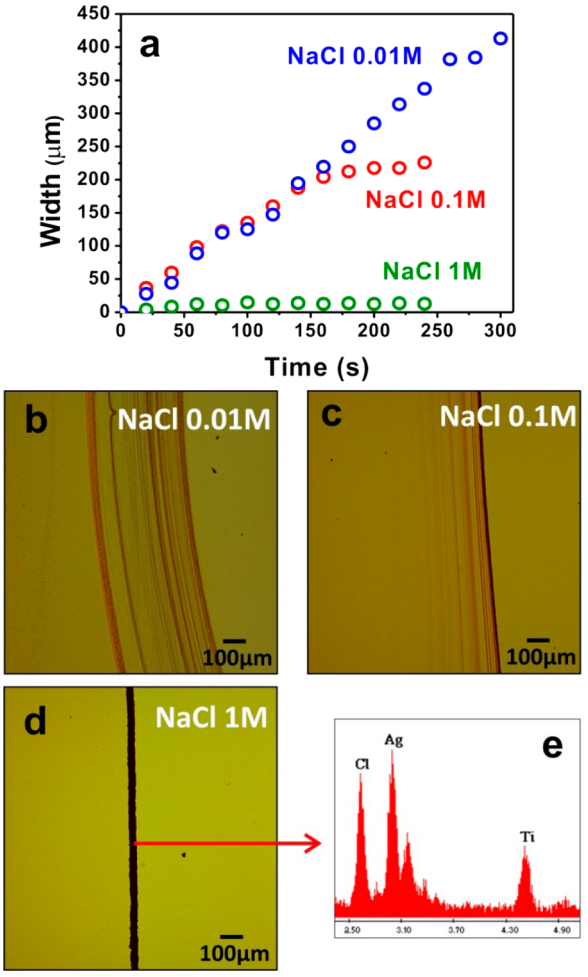


Figure 3. Localized chemistry and controlled precipitation of AgCl. (a) Width of the precipitation zone as a function of time for different NaCl concentrations, as determined from optical micrographs. Representative images of the inner pattern arising in the reaction bands for each salt concentration: (b) 0.01, (c) 0.1, and (d) 1 M. In all cases, the left side of the image corresponds to $AgNO_3$ 0.1 M. (e) EDS microanalysis showing the presence of both Ag and Cl in the reaction zone.

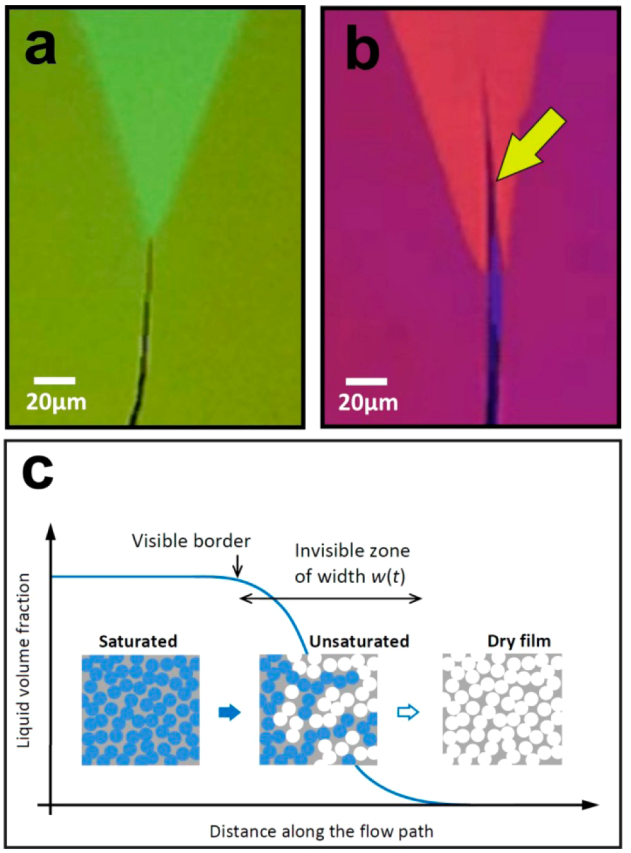


Figure 4. Early reaction. Optical microscopy images showing the chemical reaction produced in different film morphologies: (a) CLM, where precipitation occurs simultaneously with the joining of the visible border of annuli. (b) LOM, where precipitation takes place in a region of unconnected annuli (indicated by the arrow); reactants conceivably may have reached the reaction zone through the (optically invisible) unsaturated area that precedes the visible fluid border. In both cases, $AgNO_3$ 0.1 M (left) and NaCl 1 M (right) were used. (c) Drawing of the liquid volume fraction in the film as a function of distance from the drop. The visible border of the fluid front advances during infiltration, while the width of the transition zone (unsaturated) grows over time. The insets are pictorial representations of the mesoporous film in each region.

interpenetrated, and the reaction occurs throughout the zone with overlapped solutions, leading to a band of precipitated material rather than to a line (Figure 3c). Interestingly, the time required to observe a stable reaction band (around 160 s; Figure 3a) is on the order of the time required to interpenetrate the solution fronts at a distance around 240 μm, taking into account the respective infiltration rates. The case of 0.01 M NaCl solution exactly follows the trend: it presents the widest reaction band (Figure 3b) as a consequence of a more severe front broadening during infiltration, which develops a wide unsaturated zone that will gradually overlap with that of the silver solution, taking more than 450 s.

A remarkable feature that we have not mentioned yet is the inner pattern of the reaction bands, which present well-defined sub-bands that run parallel each other along the fluid front (Figures 3b and c). This composition could arise from the oscillatory behavior that exhibits the infiltration−evaporation process in mesoporous films, which was recently reported.[11] Thus, the alternating precipitation of AgCl would be produced by the alternating supply of reactants to the reaction zone with a systematic displacement in the direction of infiltration up to the point/time in which the system reaches a steady state. The resulting pattern is reminiscent of the periodic banding obtained by pH oscillations during biomorphic silica−carbonate crystallization.[24] Such oscillations have a chemical origin because a system of coupled reactions is involved. In our experiments, the underlying oscillations consist in a stepped advancement of the infiltrating fluid, which accordingly influences the precipitation reaction in the unsaturated front (see Figure 5).

It is worth adding that the reaction we are dealing with is practically instantaneous and immediately visible, which makes it possible to observe and discriminate the features described above. Nevertheless, in spite of these advantages, local precipitation may also introduce some changes in the hydrodynamic resistance of the porous matrix and partial clogging of the pore space, for example, it might influence the patterns observed in the reaction zone. Even though further experimentation is required to elucidate the origin of the complex shape of the reaction bands, at this point, it is fairly evident that the width of the reaction zone is proportional to

DOI: 10.1021/acsami.7b03080
ACS Appl. Mater. Interfaces XXXX, XXX, XXX−XXX

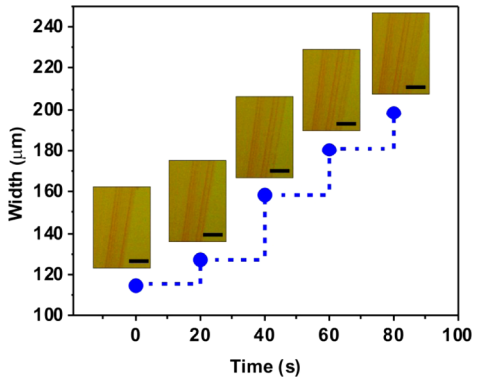


Figure 5. Stepped precipitation reaction. Schematic drawing of the precipitation zone width as a function of time according to the evolution of the intrinsic banding patterns observed through the microscope. Inset pictures are optical microscopy images illustrating the stepping behavior at the respective times. Scale bar = 100 μm.

the width w of the unsaturated area that precedes the visible liquid front. In this sense, one may observe that performing localized reactions opens new possibilities to study these complex phenomena in mesoporous films. On the other hand, these preliminary investigations suggest that films exhibiting different porosity morphologies can be utilized to handle localized chemistry, which also points to the overall versatility and robustness of the method.

CONCLUSIONS

In summary, we report a new, highly simple nanofluidic method/platform, OPN, for achieving localized chemistry on surfaces by nanofluidically handling and mixing transported reagents. Although this promising outlook of OPN included only a precipitation reaction, it could be performed on a broad range of chemical and biological reactions and enables the confined crystallization of nanomaterials at precise locations on surfaces in a spatially ordered manner. Selective functionalization/storage of mesoporous films with metal nanoparticles,[25] enzymes,[26] DNA, and other molecules[27] could also make it possible to build platforms that offer pre-existing markers for specific detection or even distance−based quantitative measurements.[28] Finally, we are optimistic that as OPN matures, it will be used to perform confined scale biological studies, enable running of high throughput sensors, and even aid in discovering novel nanostructures based on controlled synthesis.

METHODS

Film Synthesis. The technique was based on evaporation induced self-assembly following well-established protocols.[11,14,15] Crack-free mesoporous titania films were produced by dip-coating of silicon substrates at a withdrawal rate of 3 mm s^{-1} at a relative humidity (RH) of 30%. Molar ratios in the precursor sols were $TiCl_4$:EtOH:H_2O:F127 = 1:40:10:0.005. After deposition, two types of porous morphologies were obtained according to the thermal treatment. In the case of films with CLM, samples were directly calcined in air at 450 °C for 10 min by a fast-firing process. Samples with LOM were aged at 50% RH for 24 h, heated for 2 h at 60 °C and 2 h at 130 °C, and finally calcined at 450 °C for 2 h with a ramp temperature of 1 °C/min.

Film Characterization. Water adsorption−desorption isotherms were determined at 298 K by EEP[17] using a SOPRA GES5A apparatus equipped with microspot optics. Film thickness and the real component of the refractive index were obtained by fitting the ellipsometric parameters ψ (λ) and Δ (λ) in the 400−800 nm spectral range; the film refractive index was described according to a modified Cauchy equation. Film porosity was evaluated by the WinElli 2 software (Sopra Inc.), which transforms the variation of n with P/P_0 into filled pore volume using a three-medium BEMA treatment. Pore and neck size distributions were derived according to a Kelvin model. Electron microscopy images were obtained using a Zeiss LEO 982 Gemini field-emission electron microscope coupled to an X-ray microanalyzer, and transmission electron images were taken using a Philips CM200 electron microscope.

OPN-Assisted Chemical Reactions. Pairs of drops (5 μL), one of silver nitrate ($AgNO_3$) 0.1 M and the other of sodium chloride (NaCl) solutions in different concentrations, were deposited onto the mesoporous films spaced 10 mm apart. Solution infiltration and mixing zones were followed using a Mitutuyo FS70 microscope at 23 °C and 46% RH. Images were recorded using a high-resolution digital camera.

ASSOCIATED CONTENT

Supporting Information

The Supporting Information is available free of charge on the ACS Publications website at DOI: 10.1021/acsami.7b03080.

Movie S1: Localized precipitation reaction in conduit-like mesostructure (AVI)

Movie S2: Localized precipitation reaction in locally ordered mesostructure (AVI)

Sample characterization by environmental ellipsometric porosimetry (PDF)

AUTHOR INFORMATION

Corresponding Authors

*E-mail: cberli@santafe-conicet.gov.ar.

*E-mail: mbellino@cnea.gov.ar.

ORCID

Claudio L. A. Berli: 0000-0002-1321-6738

Martín G. Bellino: 0000-0002-6713-6688

Notes

The authors declare no competing financial interest.

ACKNOWLEDGMENTS

M.M. acknowledges the doctoral fellowship from CNEA, Argentina. This work was supported by CONICET (Grant PIP-0363), ANPCyT (Grants PICT-2015-1051 and PICT-2012-2969), and UNL (Grant CAI+D-78-5012011010010-0), Argentina.

REFERENCES

(1) Sparreboom, W. V.; Van Den Berg, A.; Eijkel, J. Principles and Applications of Nanofluidic Transport. *Nat. Nanotechnol.* **2009**, *4*, 713−720.

(2) Fu, J.; Schoch, R. B.; Stevens, A. L.; Tannenbaum, S. R.; Han, J. A Patterned Anisotropic Nanofluidic Sieving Structure for Continuous-flow Separation of DNA and Proteins. *Nat. Nanotechnol.* **2007**, *2*, 121−128.

(3) Guan, W.; Fan, R.; Reed, M. A. Field-effect Reconfigurable Nanofluidic Ionic Diodes. *Nat. Commun.* **2011**, *2*, 506.

(4) Huh, D.; Mills, K.; Zhu, X.; Burns, M. A.; Thouless, M.; Takayama, S. Tuneable Elastomeric Nanochannels for Nanofluidic Manipulation. *Nat. Mater.* **2007**, *6*, 424−428.

(5) Koltonow, A. R.; Huang, J. Two-dimensional Nanofluidics. *Science* **2016**, *351*, 1395−1396.

(6) Miller, O. J.; Bernath, K.; Agresti, J. J.; Amitai, G.; Kelly, B. T.; Mastrobattista, E.; Taly, V.; Magdassi, S.; Tawfik, D. S.; Griffiths, A. D. Directed Evolution by In vitro Compartmentalization. *Nat. Methods* **2006**, *3*, 561−570.

(7) Kang, S.; Douglas, T. Some Enzymes Just Need a Space of Their Own. *Science* **2010**, *327*, 42−43.

DOI: 10.1021/acsami.7b03080
ACS Appl. Mater. Interfaces XXXX, XXX, XXX−XXX

(8) Whitesides, G. M. The 'Right' Size in Nanobiotechnology. *Nat. Biotechnol.* **2003**, *21*, 1161−1165.
(9) Marre, S.; Jensen, K. F. Synthesis of Micro and Nanostructures in Microfluidic Systems. *Chem. Soc. Rev.* **2010**, *39*, 1183−1202.
(10) Metzker, M. L. Sequencing Technologies - The Next Generation. *Nat. Rev. Genet.* **2010**, *11*, 31−46.
(11) Mercuri, M.; Pierpauli, K. A.; Bellino, M. G.; Berli, C. L. A. Complex Filling Dynamics in Mesoporous Thin Films. *Langmuir* **2017**, *33*, 152−157.
(12) Ceratti, D. R.; Faustini, M.; Sinturel, C.; Vayer, M.; Dahirel, V.; Jardat, M.; Grosso, D. Critical Effect of Pore Characteristics on Capillary Infiltration in Mesoporous Films. *Nanoscale* **2015**, *7*, 5371−5382.
(13) Berli, C. L. A.; Mercuri, M.; Bellino, M. G. Modeling the Abnormally Slow Infiltration Rate in Mesoporous Films. *Phys. Chem. Chem. Phys.* **2017**, *19*, 1731−1734.
(14) Soler-Illia, G.; Angelomé, P.; Fuertes, M.; Calvo, A.; Wolosiuk, A.; Zelcer, A.; Bellino, M.; Martínez, E. Mesoporous Hybrid and Nanocomposite Thin Films. A Sol−Gel Toolbox to Create Nanoconfined Systems with Localized Chemical Properties. *J. Sol-Gel Sci. Technol.* **2011**, *57*, 299−312.
(15) Soler-Illia, G. J.; Angelomé, P. C.; Fuertes, M. C.; Grosso, D.; Boissiere, C. Critical Aspects in the Production of Periodically Ordered Mesoporous Titania Thin Films. *Nanoscale* **2012**, *4*, 2549−2566.
(16) Brinker, C. J.; Lu, Y.; Sellinger, A.; Fan, H. Evaporation-Induced Self-Assembly: Nanostructures Made Easy. *Adv. Mater.* **1999**, *11*, 579−585.
(17) Boissiere, C.; Grosso, D.; Lepoutre, S.; Nicole, L.; Bruneau, A. B.; Sanchez, C. Porosity and Mechanical Properties of Mesoporous Thin Films Assessed by Environmental Ellipsometric Porosimetry. *Langmuir* **2005**, *21*, 12362−12371.
(18) Rad, M. N.; Shokri, N. Nonlinear Effects of Salt Concentrations on Evaporation from Porous Media. *Geophys. Res. Lett.* **2012**, *39*, L04403.
(19) Pitzer, K. S.; Peiper, J. C.; Busey, R. H. Thermodynamic Properties of Aqueous Sodium Chloride Solutions. *J. Phys. Chem. Ref. Data* **1984**, *13*, 1−102.
(20) Buldyrev, S. V.; Barabási, A.-L.; Caserta, F.; Havlin, S.; Stanley, H. E.; Vicsek, T. Anomalous Interface Roughening in Porous Media: Experiment and Model. *Phys. Rev. A: At., Mol., Opt. Phys.* **1992**, *45*, R8313.
(21) Dubé, M.; Rost, M.; Alava, M. Conserved Dynamics and Interface Roughening in Spontaneous Imbibition: A Critical Overview. *Eur. Phys. J. B* **2000**, *15*, 691−699.
(22) Gruener, S.; Sadjadi, Z.; Hermes, H. E.; Kityk, A. V.; Knorr, K.; Egelhaaf, S. U.; Rieger, H.; Huber, P. Anomalous Front Broadening During Spontaneous Imbibition in a Matrix with Elongated Pores. *Proc. Natl. Acad. Sci. U. S. A.* **2012**, *109*, 10245−10250.
(23) Gruener, S.; Hermes, H. E.; Schillinger, B.; Egelhaaf, S. U.; Huber, P. Capillary Rise Dynamics of Liquid Hydrocarbons in Mesoporous Silica as Explored by Gravimetry, Optical and Neutron imaging: Nano-Rheology and Determination of Pore Size Distributions from the Shape of Imbibition Fronts. *Colloids Surf., A* **2016**, *496*, 13−27.
(24) Montalti, M.; Zhang, G.; Genovese, D.; Morales, J.; Kellermeier, M.; García-Ruiz, J. M. Local pH Oscillations Witness Autocatalytic Self-Organization of Biomorphic Nanostructures. *Nat. Commun.* **2017**, *8*, 14427.
(25) Martínez, E. D.; Bellino, M. n. G.; Soler-Illia, G. J. Patterned Production of Silver−Mesoporous Titania Nanocomposite Thin Films Using Lithography-assisted Metal Reduction. *ACS Appl. Mater. Interfaces* **2009**, *1*, 746−749.
(26) Bellino, M. G.; Tropper, I.; Duran, H.; Regazzoni, A. E.; Soler-Illia, G. J. Polymerase-Functionalized Hierarchical Mesoporous Titania Thin Films: Towards a Nanoreactor Platform for DNA Amplification. *Small* **2010**, *6*, 1221−1225.
(27) Innocenzi, P.; Malfatti, L. Mesoporous Thin Films: Properties and Applications. *Chem. Soc. Rev.* **2013**, *42*, 4198−4216.
(28) Tian, T.; Li, J.; Song, Y.; Zhou, L.; Zhu, Z.; Yang, C. J. Distance-based Microfluidic Quantitative Detection Methods for Point-of-Care Testing. *Lab Chip* **2016**, *16*, 1139−1151.

DOI: 10.1021/acsami.7b03080
ACS Appl. Mater. Interfaces XXXX, XXX, XXX−XXX